



# An experimental investigation on the acoustic properties of micro-perforated panels in a grazing flow

Xiaoqi Zhang<sup>a</sup>, Cheng Yang<sup>b</sup>, Li Cheng<sup>a,\*</sup>, Penglin Zhang<sup>b</sup>

<sup>a</sup> Department of Mechanical Engineering, The Hong Kong Polytechnic University, Kowloon, Hong Kong, China

<sup>b</sup> Institute of Vibration, Shock and Noise, School of Mechanical Engineering, Shanghai Jiao Tong University, Shanghai, China

## ARTICLE INFO

### Article history:

Received 17 July 2019

Received in revised form 24 October 2019

Accepted 25 October 2019

### Keywords:

Micro-perforated panel

Grazing flow

Experimental study

Impedance formulae validation

Sound absorption behavior

## ABSTRACT

Micro-perforated panels (MPPs) are widely used for broadband sound absorptions. In the presence of flow, MPPs exhibit complex behavior, which can be characterized by their surface acoustic impedance. Compared with no-flow conditions, studies on MPPs in low-speed grazing flow, especially experimental ones, are scarce. This paper reports an experimental study on the acoustic impedance of MPPs inside a flow duct with grazing incident waves. Through comparisons with experimentally deduced impedance data under various flow velocities, the full set of acoustic impedance formulae proposed in our previous work is validated, which is further used to investigate the sound absorptions of a MPP liner with honeycomb backing. Analyses on the sound absorption coefficient curves show that the presence of the grazing flow shifts the absorption peak to a higher frequency, widens the bandwidth and alters the maximum absorption value. Different from the no-flow conditions, however, the peak frequency is found to be less sensitive to the variation of the hole diameter when a flow is present.

© 2019 Elsevier Ltd. All rights reserved.

## 1. Introduction

A Micro-perforated panel (MPP) takes the form of a thin sheet with perforated holes typically in the sub-millimeter range. With small holes in such a scale, the panel itself can provide a high acoustic resistance and a low acoustic reactance, conducive to broadband sound absorption without the need of porous materials. Acoustic properties of a MPP are usually characterized by its surface impedance, which can be readily predicted in the no-flow condition and within the linear acoustic regime [1,2]. In addition to frequency, the acoustic impedance of an MPP mainly depends on its geometrical parameters such as hole size, panel thickness and perforation ratio. Therefore, materials used to fabricate a MPP can be customized to suit any given scenario ranging from large scale buildings [3,4] to compact mechanical systems [5–7].

In many engineering applications, MPPs are exposed to grazing flows. Due to the complex interaction between the acoustic waves and the flow field within and in the vicinity of the perforation holes, the prediction of their acoustic behaviors becomes technically more challenging. The issue has been arousing great interest in acoustic community, exemplified by the persistent effort in establishing various forms of theoretical [8–12], semi-theoretical

[13,14] and empirical [15–24] tools for acoustic impedance prediction. However, it has been observed that existing acoustic impedance formulae may give inconsistent results even for the same test case [22]. Meanwhile, existing studies have been overwhelmed by cases in which the diameter of the perforation is typically around 1 mm or above, which, in a rigorous sense, is beyond the MPP range.

The research on MPPs with low-speed grazing flows under linear acoustic excitation region is scarce, as previously reviewed [25]. Among the most relevant works, one may cite Allam and Abom [19] who proposed a set of impedance formulae based on the flow Mach number and the experimental work of Malmay et al. [26]. More recently, a comprehensive numerical investigation on MPPs with grazing flow has been conducted [25], which led to the establishment of a complete set of acoustic impedance formulae through numerical experiments. However, the proposed formulae have only been compared with a very limited amount of experimental data reported in the literature [26]. In a broader sense, it is felt that the lack of sufficient experimental data on MPPs under well-controlled testing conditions is a bottleneck problem, hampering the development of the acoustic impedance prediction tools for the study of MPPs in flow. Along with this is the insufficient knowledge on the *in-situ* sound absorption of MPPs in the presence of flow as well as its impact on the practical design as effective sound absorbers.

\* Corresponding author.

E-mail address: [li.cheng@polyu.edu.hk](mailto:li.cheng@polyu.edu.hk) (L. Cheng).

The aforementioned issues motivate the present work with twofold objectives: to validate the previously proposed acoustic impedance prediction formulae; and to gain insights into the sound absorption behavior of MPPs in the presence of a grazing flow. To this end, experiments are conducted to educe the acoustic impedance data of a MPP under various flow velocities inside a flow duct using a previously developed impedance eduction technique [27]. The educed impedance data are then used to validate our previously proposed impedance formulae. Meanwhile, the effects of the grazing flow as well as those of some key parameters of a MPP absorber on the *in-situ* sound absorption coefficient of honeycomb MPP absorbers are investigated through embedding the validated impedance prediction formula into a FEM model.

**2. Impedance eduction method**

An inverse approach is used for the acoustic impedance eduction. The impedance of a liner, flushed mounted in a flow duct, can be inversely educed by minimizing the difference between the experiment results and a wave propagation model, as detailed in reference [27]. For the completeness of the paper, the eduction method is briefly recalled here.

Fig. 1 describes the system under investigation along with the Cartesian coordinate system used in the model. Incident acoustic waves propagate along the duct with a grazing flow. A locally reactive MPP absorber, with a length of  $L$ , is flush-mounted on one of

the side walls of the duct. The system is divided into three segments: a lined segment ( $0 < Z < L$ ) with uniformly distributed surface impedance and two unlined ones, upstream ( $Z < 0$ ) and downstream ( $Z > L$ ), denoted by segment 1, 2 and 3, respectively. It is assumed that the incoming grazing flow in the duct, with an average (bulk) Mach number  $M$ , is inviscid and uniform across the cross section of the duct. Harmonic acoustic waves propagating in the uniform mean flow is governed by the convected wave equation:

$$\nabla^2 p - \left( jk_0 + M \frac{\partial}{\partial z} \right)^2 p = 0 \tag{1}$$

where  $j = \sqrt{-1}$ ;  $k_0 = \omega/c_0$  is the free-space wave number;  $\omega$  the angular frequency and  $c_0$  the sound speed.

Over the rigid and unlined portion of the duct walls, the normal particle velocity vanishes, yielding either

$$\frac{\partial p}{\partial x} = 0 \tag{2}$$

or

$$\frac{\partial p}{\partial y} = 0 \tag{3}$$

on the respective parts of the duct.

Over the lined duct portion in segment 2, Ingard-Myers boundary condition is imposed, which writes

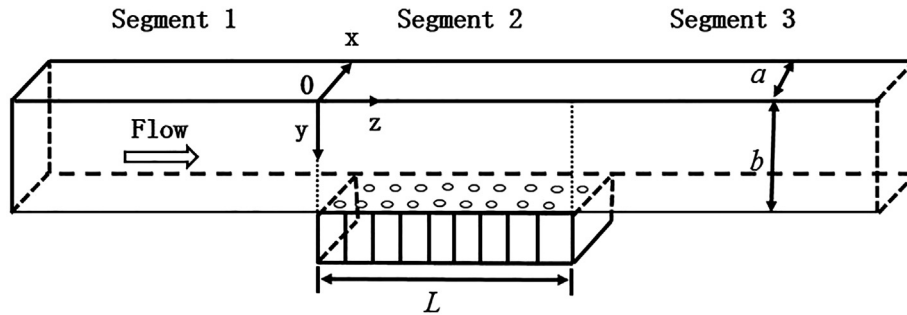


Fig. 1. Sketch of the system.



(a)



(b)

Fig. 2. Test sample (a) Honeycomb core; (b) assembled honeycomb MPP absorber.

$$jk_0 v_y(x, b, z) Z_s = \left[ jk_0 + M \frac{\partial}{\partial z} \right] p_2(x, b, z) \quad (4)$$

where  $Z_s$  is the normalized surface acoustic impedance of the liner absorber.

The acoustic pressure  $p(x, y, z)$  in different duct segments can then be expressed in the following form based on the classical mode-decomposition theory:

$$p_1(x, y, z) = \sum_N \varphi_N (A_N^+ e^{-j\alpha_N z} + A_N^- e^{-j\alpha_N z}) \quad (5)$$

$$p_2(x, y, z) = \sum_N \phi_N (B_N^+ e^{-j\beta_N z} + B_N^- e^{-j\beta_N z}) \quad (6)$$

$$p_3(x, y, z) = \sum_N \psi_N (C_N^+ e^{-j\gamma_N z} + C_N^- e^{-j\gamma_N z}) \quad (7)$$

where  $\varphi_N$ ,  $\phi_N$  and  $\psi_N$  are the  $N$ th mode shape functions of the cross section of the duct in segments 1, 2 and 3, respectively, analytically expressed as

$$\varphi_N(x, y) = \cos(k_{m1}x) \cos(k_{n1}y) \quad (8)$$

$$\phi_N(x, y) = \cos(k_{m2}x) \cos(k_{n2}y) \quad (9)$$

$$\psi_N(x, y) = \cos(k_{m3}x) \cos(k_{n3}y) \quad (10)$$

with the wave numbers in  $x$  and  $y$  directions being

$$k_{m1} = m_1 \pi / a \quad \text{and} \quad k_{n1} = m_1 \pi / b m_1, \quad n_1 = 0, 1, 2, \dots \quad (11)$$

$$k_{m2} = m_2 \pi / a, \quad m_2 = 0, 1, 2, \dots \quad (12)$$

$$k_{m3} = m_3 \pi / a \quad \text{and} \quad k_{n3} = n_3 \pi / b, \quad m_3, n_3 = 0, 1, 2, \dots \quad (13)$$

The wave number in the  $y$ -direction  $k_{n2}$  in segment 2 can be sought from the eigenvalue problem

$$-\frac{1}{Z_s} (k_0 - M \beta_N^\pm) [k_0 - M \beta_N^\pm] = j k_0 k_{n2} \tan(k_{n2} b) \quad (14)$$

The axial wave numbers  $\alpha$ ,  $\beta$  and  $\gamma$  in the three segments and their corresponding wavenumbers in the  $x$  and  $y$  directions satisfy the dispersion relation:

$$(k_x^\pm)^2 + (k_y^\pm)^2 + (k_z^\pm)^2 = (k_0 - M k_z^\pm)^2 \quad (15)$$

where the plus and minus superscripts denote waves travelling in the positive and negative  $z$  directions, respectively. The axial wavenumbers  $\alpha$  and  $\gamma$  in the unlined parts, segments 1 and 3, can be directly derived by using Eqs. (11), (13) and (15).

By defining  $A_s = \frac{1}{Z_s} A_f \eta$ , considering both  $A_s$  and  $k_{n2}$  as functions of  $\eta$  ranging from 0 (rigid) to 1 (absorber), and differentiating Eqs. (14) and (15) with respect to  $\eta$ , the following ordinary differential equation can be obtained

$$\frac{dk_{n2}}{d\eta} = \frac{A_f (k_0 - M k_z)^2}{-j k_0 \tan(k_{n2} b) - j b k_0 k_{n2} \sec^2(k_{n2} b) + 2 \eta A_f M W (k_0 - M k_z) k_{n2} / k_0} \quad (16)$$

$$W = \mp 1 / \sqrt{1 - (1 - M^2) \left[ \left( \frac{k_{m2}}{k_0} \right)^2 + \left( \frac{k_{n2}}{k_0} \right)^2 \right]} \quad (17)$$

Using the 4th order Runge-Kutta integration scheme by integrating Eq. (16) over  $\eta$  from 0 to 1, the positive and negative axial wavenumbers as well as their corresponding wave numbers in  $y$  direction in the lined part (segment 2) can then be extrapolated.

The acoustic fields in the three segments are coupled together by using the mode-matching method by ensuring the continuity of the acoustic pressure and axial particle velocity at the interface

between each pair of segments and the unknown modal amplitudes  $A$ ,  $B$  and  $C$  in Eqs. (5)–(7) can be readily obtained given that the incidence and the boundary condition at the termination of the duct are known.

The unknown liner impedance is then obtained through an iterative procedure by minimizing the following objective function,

$$F = \sum_n^N (p_{n, \text{sim}} - p_{n, \text{exp}}) (p_{n, \text{sim}}^* - p_{n, \text{exp}}^*) \quad (18)$$

where the superscript  $*$  represents the complex conjugate;  $p_{n, \text{exp}}$  and  $p_{n, \text{sim}}$  are the measured and computed sound pressure in the duct, respectively.

Considering only plane wave can propagate in the unlined downstream segment for the present study, the reflection effect of the termination of the duct is included by introducing the reflection coefficient only for the plane wave mode, as  $R_0 = \frac{C_0}{C_0}$ , which can be obtained by two microphones flushed mounted in the downstream unlined part of the duct.

### 3. Measurements

#### 3.1. Test sample

The test sample is a single layer MPP absorber consisting of a micro-perforated panel, a honeycomb core and an aluminum backing plate as shown in Fig. 2. The edges of the absorber are carefully sealed to avoid acoustic leakage. The sample is designed to have a maximum sound absorption near 1200 Hz, below the cut-on frequency of the flow duct. The MPP, made of aluminum, has a dimension of  $500 \times 100$  mm with cylindrical holes manufactured through chemical corrosion. The holes are manufactured to be uniformly distributed over the sample surface. The perforated ratio of the panel is 0.945%. Both the diameter of the hole and the thickness of the panel are 0.5 mm. The honeycomb core is made of ABS resin, forming a backing layer of 25 mm thick. It is designed and 3D printed to ensure that the center of each honeycomb cell is coaxially aligned with a MPP hole. The honeycomb core is bonded to the MPP to rigidify the thin panel and make the MPP absorber locally reactive [28].

#### 3.2. Experimental set-up

Measurements are conducted in a closed-loop low-speed acoustic wind tunnel with a background noise of around 82 dB at the maximum flow speed (22 m/s) considered in the current study. The working section is about 1.8 m long with a cross section of  $100 \times 100$  mm, corresponding to a cut-on frequency of 1700 Hz. As shown in Figs. 3 and 4, the honeycomb MPP absorber is flush-mounted on the upper wall of the square duct within its working section. Eleven 1/4-inch microphones (B&K 4935) are used to measure the acoustic pressure at different locations along the duct. They are flush-mounted on the wall of the duct opposite to the absorber and connected to conditioning amplifiers (B&K Nexus 2691). The positions and the separation distance between the microphones are shown in Fig. 3. A single-tone acoustic excitation generated by a loudspeaker is used as the sound source within the frequency range below the cut-off frequency of the duct, thus allowing the sample to be exposed to a grazing plane wave excitation. Microphone 1 is used to monitor the sound pressure of the acoustic source. Preliminary tests are made to ensure the linear property of the MPP absorber by varying the incidence pressure levels up to 130 dB. In the subsequent analyses, test cases using pure tone excitation at 110 dB, are used to make sure the results presented in this work are in a range where the MPP behave lin-

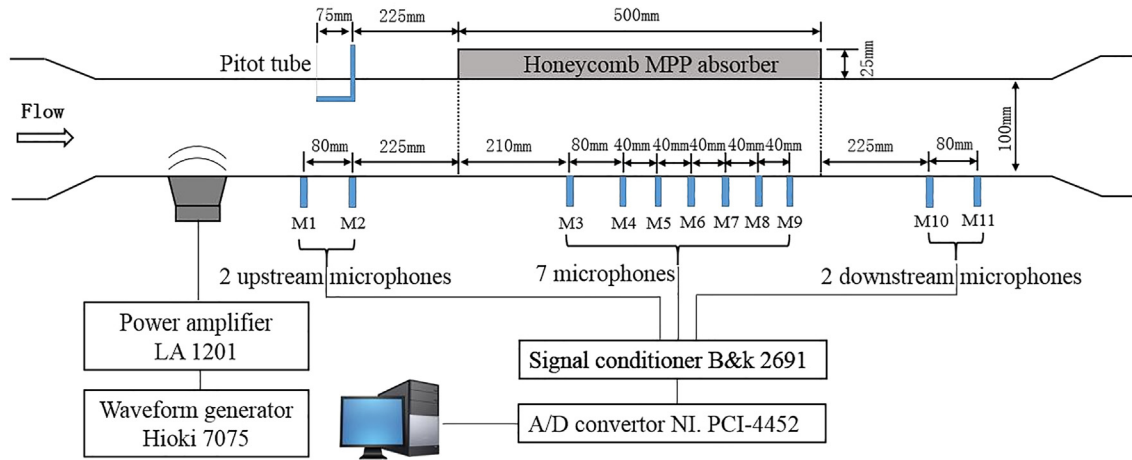


Fig. 3. Sketch of the test setup for eduction of the acoustic impedance of a MPP liner.

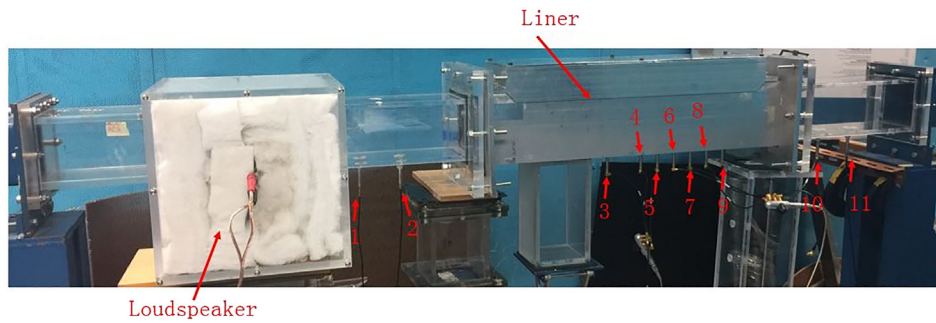


Fig. 4. Experimental setup for eduction of the acoustic impedance of a MPP liner.

early. The middle span flow profile, upstream the absorber, is obtained by measuring the axial velocities at different positions in the normal wall direction through moving a pitot tube transversely across the duct.

Prior to the impedance eduction tests, microphones are calibrated to guarantee the quality of the measured data. As shown in Fig. 5, two microphones are closely mounted in the duct opposite to each other, whose outputs are used to calibrate the pressure amplitude and phase. For the calibration, the central portion of the duct are closed by rigid caps.

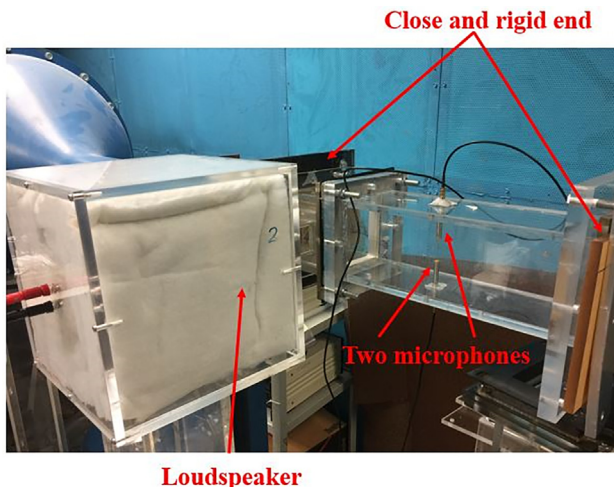


Fig. 5. Setup for microphone calibrations.

## 4. Results and discussions

### 4.1. Mean flow profile in the duct

For a fully developed flow in a duct, the following well-adopted equations [29] can be used to calculate the mean streamwise velocity.

$$u^+ = y^+ \text{ for } y^+ < 5 \text{ in viscous sublayer} \quad (19)$$

$$u^+ = \frac{1}{0.41} \ln y^+ + 5.2 \text{ for } \frac{y}{e} < 0.1 \text{ in the inner flow region} \quad (20)$$

$$\frac{\bar{u} - \bar{u}_{cl}}{u_\tau} = 0.008 \left(\frac{y}{e}\right)^{-2.76} \text{ for } \frac{y}{e} > 0.1 \text{ for in the outer flow region} \quad (21)$$

where  $u^+ = \bar{u}/u_\tau$ ,  $y^+ = yu_\tau/\nu$ ,  $\bar{u}$  is the mean streamwise velocity,  $\bar{u}_{cl}$  is the centerline velocity,  $u_\tau$  is the friction velocity and  $e$  is the half channel height.  $u_\tau$  can be calculated by

$$u_\tau = u_\infty \sqrt{\frac{\lambda}{8}} \quad (22)$$

$$\lambda = \frac{0.178}{R_e^{1/5}} \quad (23)$$

in which  $u_\infty$  is the free-stream velocity of the incoming flow,  $\lambda$  is the Darcy friction factor proposed by Fujita [30] for a square duct. Reynolds number  $R_e = \frac{hu_\infty}{\nu}$ , with  $h$  being the height of the square duct.

The inner flow region described by Eqs. (19) and (20) is universal and independent of the channel geometry. However, the geometry of the channel is important to the outer flow region described by Eq. (21), which here is interpolated from the experimental data. The measured mean stream-wise velocity profiles, upstream the MPP absorber, for different average flow Mach numbers are shown in Fig. 6, along with the theoretically calculated profiles. The good agreement between the two sets of data confirms the full development of the flow and also verifies the averaged Mach numbers calculated from the measured data.

#### 4.2. Measured and predicted MPP acoustic impedance

The previously proposed formulae [25], for the prediction of the acoustic impedance of MPPs with grazing flow, are compared with the educed impedance data.

The normalized acoustic impedance of MPPs with grazing flow is written as

$$Z_{flow} = R_{flow} + j\chi_{flow} \quad (24)$$

where  $R_{flow}$  and  $\chi_{flow}$  are the normalized acoustic resistance and reactance of the MPPs, respectively, detailed as

$$R_{flow} = R_{in} + \left[ 0.0356 \left( \frac{t}{d} \right)^{-3.236} + 0.0157 \right] \frac{Gt}{\delta c_0} + \left[ 1.369 - 2.331 \left( \frac{t}{d} \right)^{-2.195} \right] \frac{fd}{\delta c_0} \quad (25)$$

$$\chi_{flow} = \frac{\omega}{\delta c_0} \left[ t + \varepsilon \frac{8d}{3\pi} \right]$$

$$\varepsilon = (1 + 0.6t/d) \exp \left[ -(\sqrt{Gv}/ft - 0.12d/t)/(0.25 + t/d) \right] - 0.6t/d \quad (26)$$

In the above expressions,  $R_{in} = \frac{32v\omega}{\delta c_0 d^2} \left[ 1 + \frac{K^2}{32} \right]^{\frac{1}{2}}$ ;  $K = d\sqrt{\omega/4\nu}$ ;  $t$  is the thickness of the panel;  $d$  the diameter of the hole;  $\delta$  the perforated ratio of the panel;  $f$  the frequency and  $\nu$  the kinematic viscosity of the air.  $G$  is the velocity gradient in the viscous sublayer, which can be calculated by

$$G = \frac{u_{\infty}^2 \lambda}{8\nu} \quad (27)$$

It is relevant to note that the above impedance formulae use the velocity gradient in the viscous sublayer over the duct wall as the key parameter to characterize the flow effect. The resistance part is

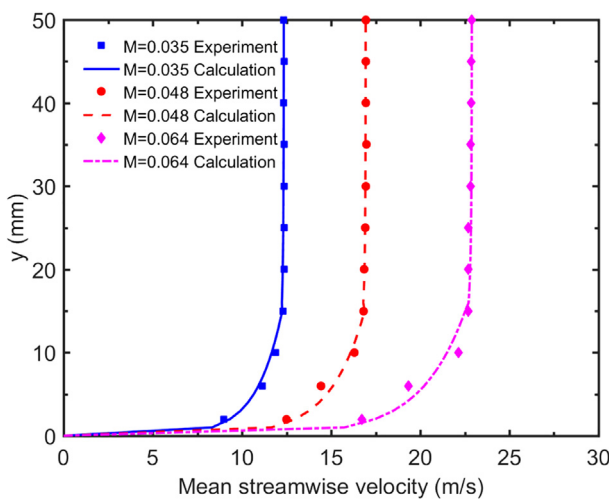


Fig. 6. Mean flow profiles upstream the liner at different flow velocities.

obtained through curve fitting a large amount of CFD simulation data under various flow and acoustic conditions, whilst the reactance part is taken from Cummings [21] after being cast in terms of  $G$ . The proposed formulae have been validated in our previous work [25] through comparisons with the experimental data reported in reference [26]. However, as the published experimental data on MPPs with grazing flow are scarce and limited to some very specific test configurations, we will use the educed experimental impedance data under various flow velocities to provide further validation of the proposed impedance formulae.

Fig. 7 shows the comparison of the acoustic impedance between the results predicted by the proposed impedance formulae and the experimentally educed data at different flow speeds, corresponding to three different Mach numbers. The comparison shows acceptable agreement between the two sets of results. Discrepancies on the resistance observed at low frequencies are mainly due to the limited length of the liner with respect to the acoustic wavelength to support the impedance eduction process [31]. Meanwhile, when approaching the cut-on frequency, the non-planary nature of the acoustic waves start to gradually show, which may also partly explain the deviation at the high frequency end of the curves. Nevertheless, the comparison indicates that although the acoustic resistance prediction formula is established based on CFD generated data through numerical experiments in a relatively ideal environment, a reasonable agreement between the prediction results and experimental data at various flow speeds can still be observed. As to the reactance part, the formula developed by Cummings [21] can give reasonably good agreement with the experimental data as well. It is worth noting that the experiments were designed and carried out in accordance with the validation range of the proposed impedance formulae, specified in [25]. As to other more complex cases which go beyond the flow-duct configuration or the pre-defined application range [25] like flow with a higher Reynolds number over an open space, further investigations are needed to assess the applicability of the proposed impedance formula.

#### 4.3. Measured and predicted sound absorption coefficient

The validated impedance formulae are used to study the *in-situ* sound absorption behavior of MPP absorbers with grazing flow. The sound absorption coefficient  $\alpha$  is defined as the fraction of the sound power absorbed by the MPP absorber over the injected sound power when an incident plane wave is transmitted through the duct, which writes

$$\alpha = \frac{\Pi_{in} - \Pi_{out} - \Pi_{reflect}}{\Pi_{in}} \quad (28)$$

where

$$\Pi_{in} = \frac{|p_i|^2}{2\rho_0 c_0} S \quad (29)$$

$$\Pi_{reflect} = \frac{|p_r|^2}{2\rho_0 c_0} S \quad (30)$$

are the incident and reflected sound power in segment 1, respectively. In Eqs. (29) and (30),  $S$  is the cross-section area of the duct,  $|p_i|$  and  $|p_r|$  are the pressure amplitude of the incident and reflected waves in segment 1, respectively, which can be obtained from two upstream microphones (M1 and M2 in Fig. 3) by using model-decomposition method.

The transmitted sound power can be derived by

$$\Pi_{out} = \frac{\Pi_{in}}{10^{TL/10}} \quad (31)$$

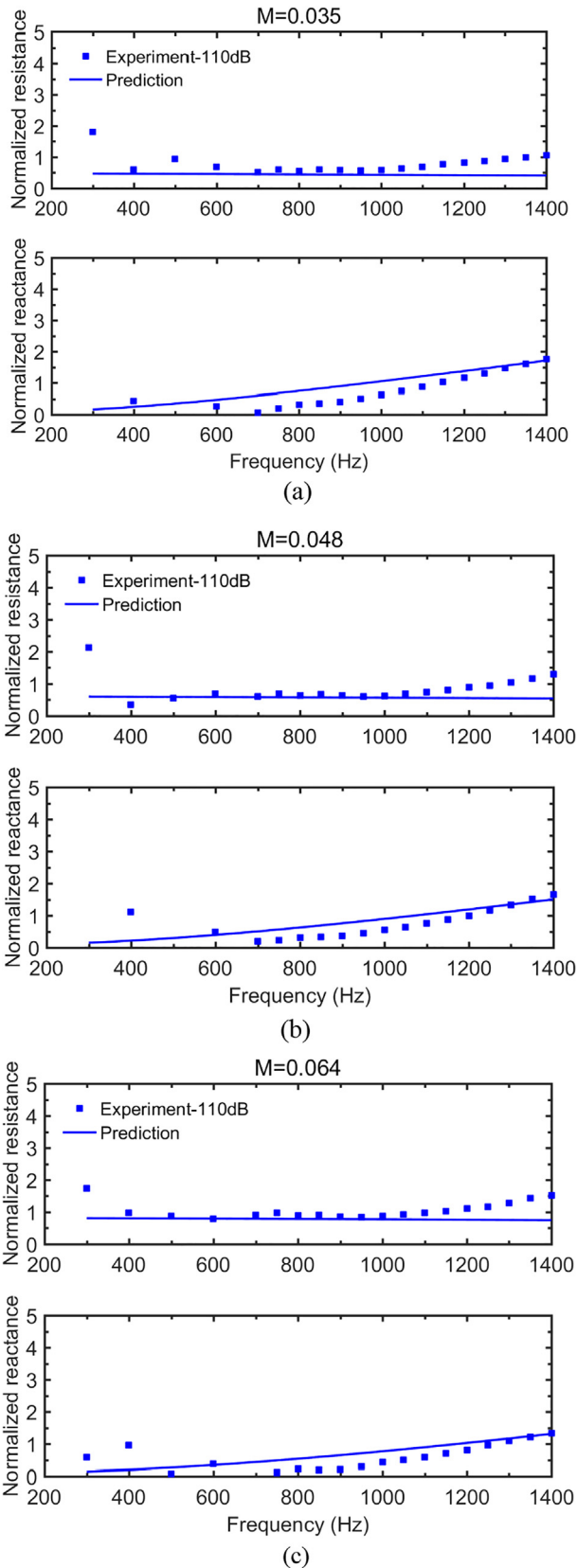


Fig. 7. Comparisons of the acoustic impedance obtained from the prediction formulae and experiments at different flow velocities.

where  $TL = 10 \log_{10} \frac{\prod_{in}}{\prod_{out}}$  is the transmission loss measured by using the two source method [32].

A 3D finite element method is employed for the sound absorption coefficient calculation. In view of the low flow speed in the duct, the convective effect on the wave propagation in the duct is neglected [7]. Therefore, the acoustic medium itself is considered to be still and the grazing flow effects are included in the acoustic impedance of MPPs by using the aforementioned validated formulae. The entire honeycomb MPP liner used in the model is treated through introducing a surface impedance described by  $Z_s = Z_{flow} - j \cot(k_0 D)$ , where  $D$  is the depth of the backing cavity. Eqs. (29) and (30) are still used to calculate the incident and reflected sound power. However, considering the non-reflective boundary condition at the end of the duct in the finite element model, the transmitted sound power is calculated by

$$\prod_{out} = \frac{|p_{11}|^2}{2\rho_0 c_0} S \quad (32)$$

where  $|p_{11}|$  is the calculated pressure amplitude of the point M11, as shown in Fig. 3.

For comparisons, the conventionally used equivalent electric circuit method is also employed to calculate the sound absorption coefficient as,

$$\alpha = \frac{4\text{Real}(Z)}{(1 + \text{Real}(Z))^2 + (\text{Imag}(Z) - \cot(\omega D/c_0))^2} \quad (33)$$

where  $Z$  is the normalized acoustic impedance of MPPs.

Comparisons of the experimentally measured and FEM predicted sound absorption coefficients of the honeycomb MPP liner are depicted in Fig. 8. The results show good agreement between the FEM prediction and the measured data at various flow speeds in terms of the maximum absorption value, bandwidth and the location of peak frequency. These comparisons provide additional evidence that the acoustic impedance prediction formulae established in our previous work is valid and can be used to predict the acoustic performance of the MPP absorbers with grazing flow. Also shown in the figure are the absorption coefficient curves predicted by the equivalent circuit method where a considerable discrepancy, in terms of both the resonance frequency and absorption value, can be noticed. This is somehow expected due to two factors: first, the equivalent circuit model considers normal acoustic incidence, which is obviously different from the grazing case considered here; second, the liner in the duct is of finite size in the stream-wise dimension. The acoustic scattering due to the impedance discontinuity at the junctions between the lined and rigid walls gives rise to an acoustic field different from that for the stream-wise infinite case. Such an influence generally decreases with the increase of the liner length. In summary, the result in Fig. 8 implies that the absorption coefficient formulae which is commonly used in building acoustics cannot accurately estimate the absorption performance of an MPP absorber in a duct and the consideration of full set of the flow duct with the proposed acoustic impedance formulae is necessary.

## 5. Parametric studies

The absorption coefficient of a MPP absorber depends on multiple parameters such as the hole diameter, panel thickness, perforation ratio, cavity depth and grazing flow speed. Without flow, the influence of these parameters on the sound absorption coefficient is well established. This is not the case when a flow is present due to the very limited research on MPPs with grazing flow. Hereafter, parameter studies are carried out by using the validated impedance formulae and the finite element method to revisit these issues.

The normalized acoustic impedance and the corresponding sound absorption coefficient of the honeycomb MPP absorber at

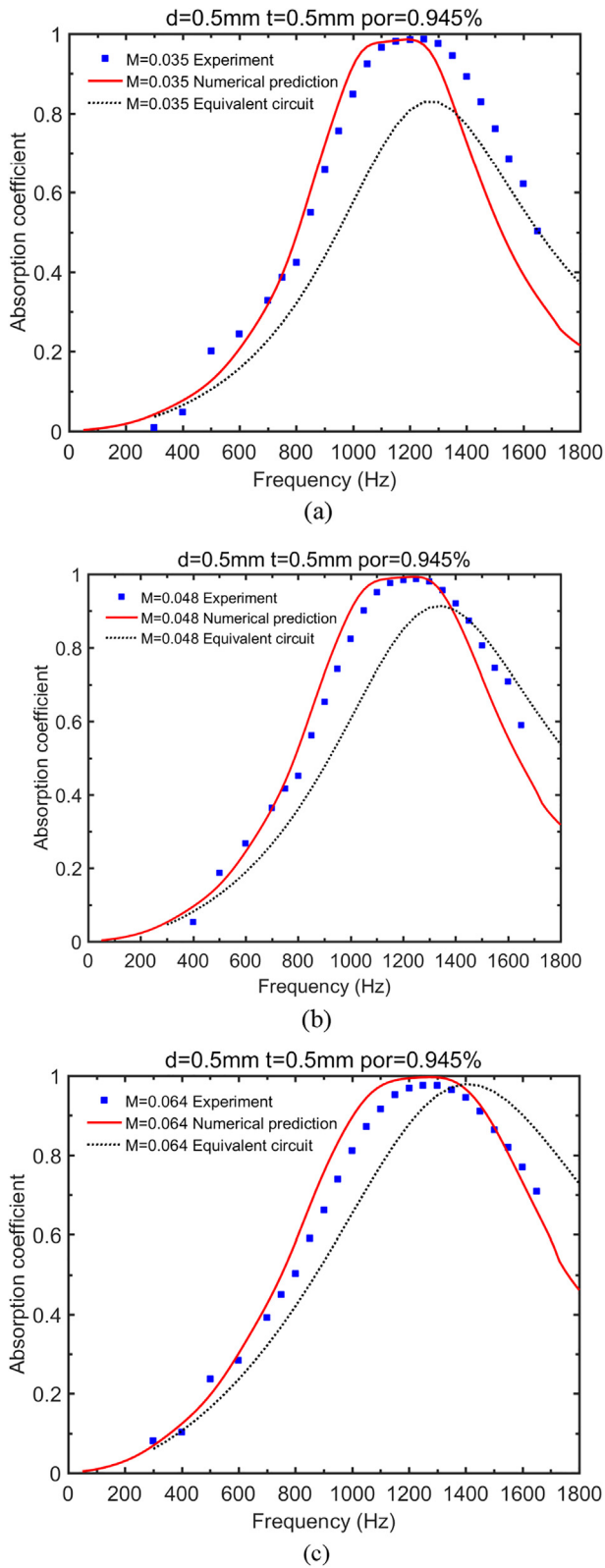


**Fig. 8.** Comparisons of the sound absorption coefficient among numerical predictions, the equivalent electric circuit method and the experimental data at different flow velocities.

different flow velocities are plotted and compared in Fig. 9. It can be seen from Fig. 9a that in the presence of grazing flow, the resistance is nearly constant in the entire frequency range while the

reactance increases with the frequency. In addition, the mean flow velocity strongly affects both the resistance and the reactance of the MPP. With the increase of the grazing flow speed, the resistance curve is elevated across the frequency spectrum while the slope of the reactance curve decreases. One possible explanation for this grazing flow effects is that the viscous effect in the hole is enhanced and the acoustic mass in the hole is “blown away” due to the presence of the grazing flow [9].

Fig. 9b depicts the absorption coefficient of the MPP absorber for different flow speeds. It is observed that the increase of grazing flow speed shifts the absorption peak to a higher frequency, widens the absorption bandwidth and alters the maximum value of the absorption. The changes in the absorption coefficient curve are attributed to the change in both the resistance and the reactance of the MPP. On one hand, the reduction in the reactance shifts the peak absorption to a higher frequency. On the other hand, the increase in the resistance generally yields a broader absorption band [2]. Meanwhile, the value of the resistance approaches to one and then drowels away, leading to a first increase and then a decrease in maximum value.

The influence of the MPP hole diameter on the absorption coefficient with grazing flow is examined in Fig. 10a by keeping the perforated ratio and the panel thickness constant. It can be seen

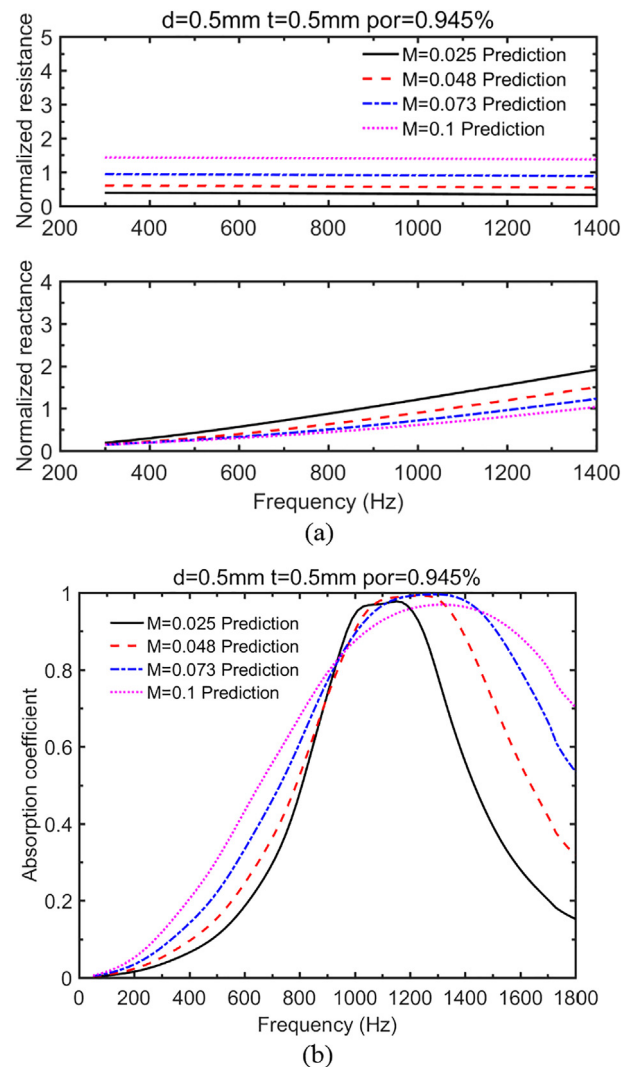


**Fig. 9.** (a) Normalized acoustic impedance, (b) Sound absorption coefficient under different flow velocities.

that the sound absorption bandwidth decreases with the increase of the hole diameter but the location of the peak frequency is nearly invariant with the hole diameter in the presence of grazing flow. This is different from the no-flow case where an increase in the hole diameter increases the air mass in the hole and consequently shifts the maximum absorption to low frequencies. As illustrated in Fig. 10b, the acoustic reactance (mass) is insensitive to the variation of the hole diameter when a flow is present. As a result, absorption peaks occur around the same frequency.

The effect of the panel thickness is shown in Fig. 11, where the hole diameter (0.5 mm) and the perforated ratio of the MPPs (0.945%) are kept constant. Results indicate that in the presence of the grazing flow, an increase in the panel thickness shifts the absorption peak to a lower frequency and alters the maximum sound absorption value. However, the absorption bandwidth is nearly unchanged with respect to the panel thickness. These phenomena can be attributed to the fact that the increase in the panel thickness enhances the viscous dissipation and increases the acoustic mass in the hole and finally leads to the variations of the peak frequency and the maximum value.

Fig. 12 shows a comparison of the sound absorption coefficient between different absorbers with different perforation ratios but

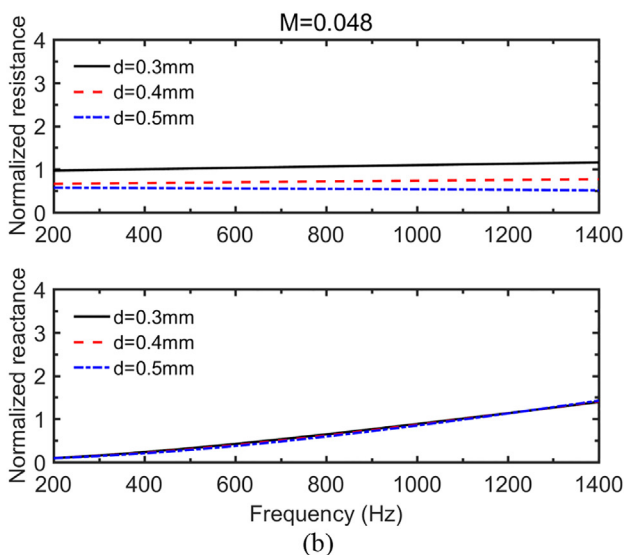
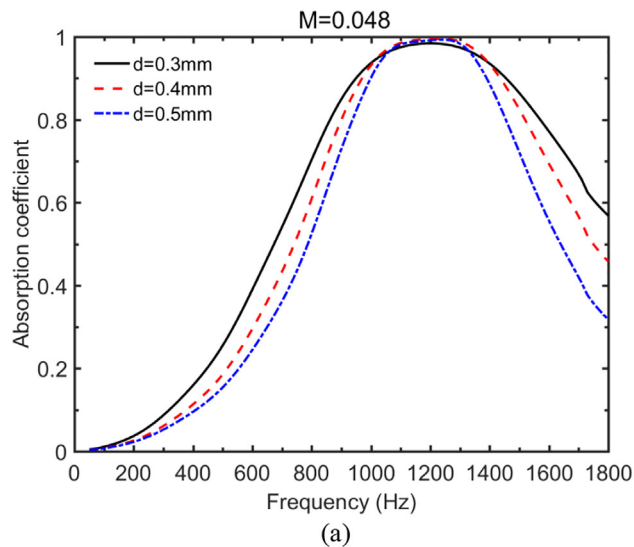


Fig. 10. (a) Absorption coefficients, (b) Normalized acoustic impedance with different hole diameters.

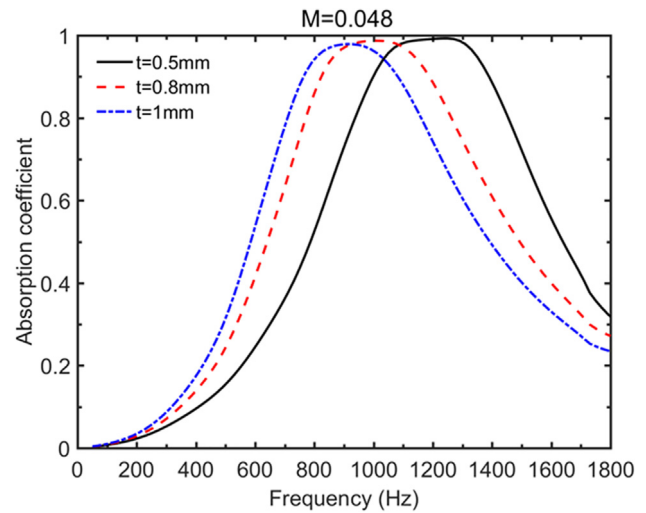


Fig. 11. Absorption coefficients with different thicknesses of the panel.

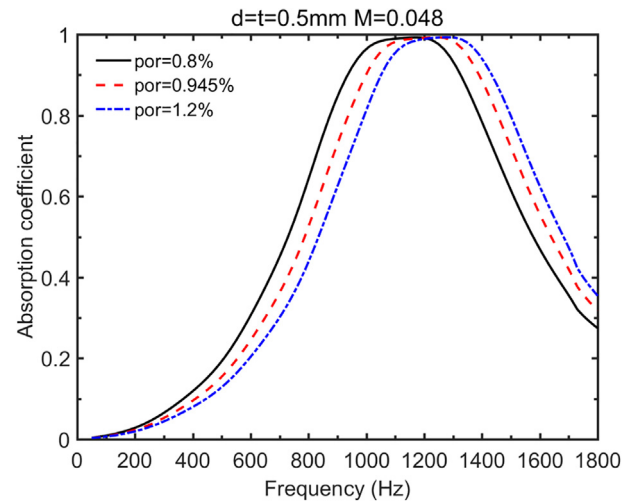


Fig. 12. Absorption coefficients with different perforated ratios.

the same hole diameter and panel thickness. It can be seen that, with the grazing flow, an increase in the perforation ratio shifts the peak absorption to a higher frequency while the absorption bandwidth is insensitive to the perforation ratio.

From the above analyses, it can be seen that the *in-situ* acoustic performance of MPPs with flow depends on the full set of MPP and flow parameters in a less intuitive manner. The changes of these parameters can provide considerable rooms for the tuning of desired MPP absorbers based on need. As the grazing flow can broaden the bandwidth, generally, with appropriate panel thickness and perforated ratio, holes with a smaller diameter in the presence of grazing flow can help achieve sound absorption with a broader bandwidth.

## 6. Conclusions

The acoustic behavior of Micro-perforated panels exposed to a fully developed grazing flow is investigated both experimentally and numerically. An inverse impedance eduction method is employed to experimentally obtain the acoustic impedance of a MPP under low-speed grazing flow within a linear acoustic excitation region. Using the measured data, the consistency and the

accuracy of a complete set impedance prediction formulae established in our previous work are validated. Combining the validated impedance prediction formulae with a 3D FEM model, grazing flow effects on the sound absorption coefficient of honeycomb MPP absorbers inside a flow duct are investigated. Results show that increasing the grazing flow speed shifts the absorption peak to a higher frequency, widens the absorption bandwidth and alters the maximum absorption value. While the thickness and the perforation ratio effects remain the same, the maximum absorption frequency shows no obvious dependence on the hole diameter variation in the presence of grazing flow.

### Declaration of Competing Interest

The authors declare that they have no known competing financial interests or personal relationships that could have appeared to influence the work reported in this paper.

### Acknowledgement

The authors thank the support from Research Grant Council of the Hong Kong SAR (PolyU 152036/18E).

### Appendix A. Supplementary data

Supplementary data to this article can be found online at <https://doi.org/10.1016/j.apacoust.2019.107119>.

### References

- [1] Maa DY. Theory and design of microperforated panel sound-absorbing constructions. *Sci Sinica* 1975;18(1):55–71.
- [2] Maa DY. Potential of microperforated panel absorber. *J Acoust Soc Am* 1998;104(5):2861–6.
- [3] Kang J, Brocklesby M. Feasibility of applying micro-perforated absorbers in acoustic window systems. *Appl Acoust* 2005;66(6):669–89.
- [4] Yu WZ. Design and noise reduction of elevated road barrier of micro-perforated panels with linear-change cavity. *Environ Pollut Control* 2008;7:67–9.
- [5] Li G, Mechefske CK. A comprehensive experimental study of micro-perforated panel acoustic absorbers in mri scanners. *Magn Reson Mater Phys Biol Med* 2010;23(3):177–85.
- [6] Yang C, Cheng L. Sound absorption of microperforated panels inside compact acoustic enclosures. *J Sound Vib* 2016;360:140–55.
- [7] Allam S, Abom M. A new type of muffler based on microperforated tubes. *J Vib Acoust* 2011;133(3):031005.
- [8] Rice EJ. Theoretical study of the acoustic impedance of orifices in the presence of a steady grazing flow. *J Acoust Soc Am* 1976;59(5):S32.
- [9] Ronneberger D. The acoustical impedance of holes in the wall of flow ducts. *J Sound Vib* 1972;24(1):133–50.
- [10] Howe M, Scott M, Sipic S. The influence of tangential mean flow on the rayleigh conductivity of an aperture. *Proc R Soc Lond A Mathemat Phys Eng Sci* 1996;452(1953):2303–17. The Royal Society.
- [11] Jing X, Sun X, Wu J, Meng K. Effect of grazing flow on the acoustic impedance of an orifice. *AIAA J* 2001;39(8).
- [12] Walker B, Charwat A. Correlation of the effects of grazing flow on the impedance of helmholtz resonators. *J Acoust Soc Am* 1982;72(2):550–5.
- [13] Hersch A, Walker B. Effect of grazing flow on the acoustic impedance of helmholtz resonators consisting of single and clustered orifices. *J Acoust Soc Am* 1982;72(2):642.
- [14] Rogers T, Hersh A. "The effect of grazing flow on the steady state resistance of square-edged orifices," in Proceedings of the Second AIAA Aeroacoustics Conference, 1976.
- [15] Phillips B. "Effects of high-wave amplitude and mean flow on a helmholtz resonator," 1968.
- [16] Bauer AB. Impedance theory and measurements on porous acoustic liners. *J Aircr* 1977;14(8):720–8.
- [17] Dean L. "Coupling of helmholtz resonators to improve acoustic liners for turbofan engines at low frequency," 1975.
- [18] Elnady T, Bodén H. "An inverse analytical method for extracting liner impedance from pressure measurements. in Proceedings of the 10th AIAA/CEAS Aeroacoustics Conference, Manchester, UK, May, 2004, pp. 10–12.
- [19] Allam S, Abom M. Experimental characterization of acoustic liners with extended reaction. In The 14th AIAA/CEAS Conference, 2008, vol. 3074.
- [20] Kooi J, Sarin S. An experimental study of the acoustic impedance of helmholtz resonator arrays under a turbulent boundary layer, in AIAA, Astrodynamic Specialist Conference, 1981.
- [21] Cummings A. The effects of grazing turbulent pipe-flow on the impedance of an orifice. *Acta Acust Unit Acust* 1986;61(4):233–42.
- [22] Kirby R, Cummings A. The impedance of perforated plates subjected to grazing gas flow and backed by porous media. *J Sound Vib* 1998;217(4):619–36.
- [23] Dickey N, Selamet A, Ciray M. An experimental study of the impedance of perforated plates with grazing flow. *J Acoust Soc Am* 2001;110(5):2360–70.
- [24] Lee S-H, Ih J-G. Empirical model of the acoustic impedance of a circular orifice in grazing mean flow. *J Acoust Soc Am* 2003;114(1):98–113.
- [25] Zhang X, Cheng L. Acoustic impedance of micro-perforated panels in a grazing flow. *J Acoust Soc Am* 2019;145(4):2461–9.
- [26] Malmay C, Carbonne S, Auregan Y, Pagneux V. "Acoustic impedance measurement with grazing flow," in AIAA Conference Paper, 2001.
- [27] Yang C, Fang Y, Zhao C, Zhang X. On modeling the sound propagation through a lined duct with a modified ingard-myers boundary condition. *J Sound Vib* 2018;424:173–91.
- [28] Yang C, Cheng L, Hu Z. Reducing interior noise in a cylinder using micro-perforated panels. *Appl Acoust* 2015;95:50–6.
- [29] Pope SB. *Turbulent flows*. IOP Publishing; 2001.
- [30] Fujita H. Turbulent flow in smooth and rough-walled square ducts. *Trans Jpn Soc Mech Eng Ser B* 1979;45:197–207.
- [31] Jones MG, Watson WR, Howerton BM, Busse-Gerstengarbe S. "Comparative study of impedance reduction methods, part 2: Nasa tests and methodology," in 19th AIAA/CEAS Aeroacoustics Conference, 2013, p. 2125.
- [32] Munjal M, Doige A. Theory of a two source-location method for direct experimental evaluation of the four-pole parameters of an aeroacoustic element. *J Sound Vib* 1990;141(2):323–33.